ORGANIC CHEMISTRY

Total synthesis of himastatin

Kyan A. D'Angelo[1], Carly K. Schissel[1], Bradley L. Pentelute[1,2,3,4]*, Mohammad Movassaghi[1]*

The natural product himastatin has an unusual homodimeric structure that presents a substantial synthetic challenge. We report the concise total synthesis of himastatin from readily accessible precursors, incorporating a final-stage dimerization strategy that was inspired by a detailed consideration of the compound's biogenesis. Combining this approach with a modular synthesis enabled expedient access to more than a dozen designed derivatives of himastatin, including synthetic probes that provide insight into its antibiotic activity.

The proliferation of multidrug-resistant pathogenic bacteria is widely recognized as a threat to global health (*1*, *2*). Natural products have served as the primary inspiration for new antibiotics to treat bacterial infections (*3*). (–)-Himastatin (**1**) is a macrocyclic peptide with a homodimeric structure isolated from *Streptomyces himastatinicus* (Fig. 1) that demonstrates antibiotic and antitumor activity (*4*–*6*). Although (–)-himastatin's (**1**) mechanism of action is not known, an early investigation demonstrated that its antibiotic activity was reduced in the presence of sodium salts of phospholipids and fatty acids, leading to speculation that (–)-himastatin (**1**) may target the bacterial membrane (*7*). (–)-Himastatin's (**1**) homodimeric structure does not resemble those of any well-characterized antibiotic class, including known membrane-disrupting cyclic peptides. The most distinctive structural feature of (–)-himastatin (**1**) is the central C5–C5′ linkage between cyclotryptophan residues that is formed in the final biosynthetic step (*8*) and is critical for the observed Gram-positive antibiotic activity (*9*). Related monomeric natural products discovered after (–)-himastatin (**1**), including (–)-NW-G01 (**S2**), show a substantial enhancement in antibiotic activity upon chemoenzymatic dimerization (*10*) (fig. S1). Other notable structural features of (–)-himastatin (**1**) include the alternating sequence of D- and L-amino acids, a depsipeptide linkage, and the piperazic acid residue with γ-hydroxylation.

Danishefsky's landmark synthesis of (–)-himastatin (**1**), which clarified the Cα stereochemistry of the cyclotryptophan residue, featured an early-stage Stille coupling to form the central C5–C5′ linkage followed by bidirectional elaboration of a dimeric cyclotryptophan (*9*). Early-stage formation of this linkage also featured in total syntheses of the related natural product (–)-chloptosin (**S1**) by Yao (*11*) and Ley (*12*) and their co-workers, who found that cross-coupling approaches to achieve a more attractive late-stage dimerization (which would also offer access to heterodimeric derivatives) were not successful (*12*). Motivated by the distinctive structure, established synthetic challenge, and antibiotic activity, we became interested in developing a concise total synthesis of (–)-himastatin (**1**) that would offer rapid access to derivatives for chemical biology studies.

The key unaddressed challenge of uniting two complex fragments to form the C5–C5′ bond at the center of (–)-himastatin's (**1**) dimeric structure encouraged us to consider the development of a new synthetic methodology. To address the C_{sp2}–C_{sp2} linkage present in (–)-himastatin (**1**), we needed to identify a strategy that stands apart from our group's prior approaches based on reductive or photolytic radical generation and coupling to secure C_{sp3}–C_{sp3} linkages and C_{sp3}–C_{sp2} linkages between similar (*13*) and dissimilar fragments (*14*). We began with a detailed examination of (–)-himastatin's (**1**) biosynthesis from a linear peptide **4** that is cyclized and then subjected

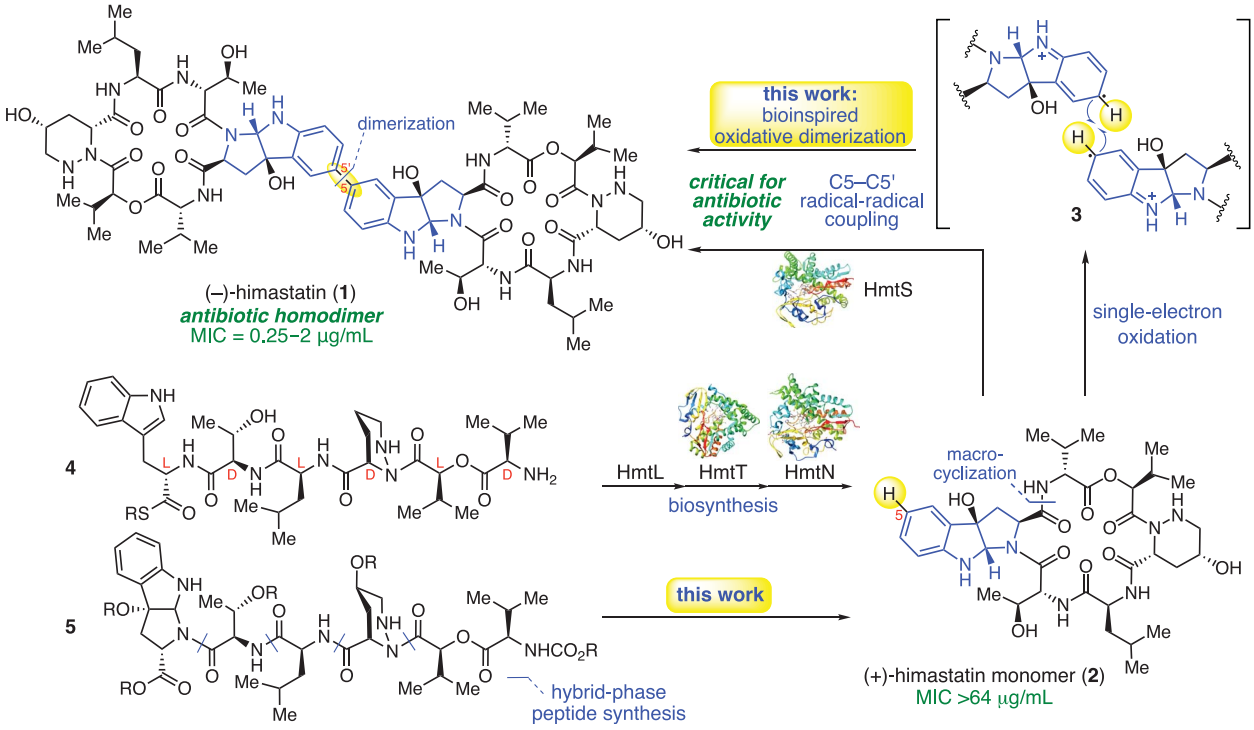

Fig. 1. Comparison of the biogenesis of himastatin and our bioinspired synthetic strategy. MIC values for (–)-himastatin (**1**) are taken from (*4*) against Gram-positive bacteria. MIC, minimum inhibitory concentration. Protein Data Bank identification codes: HmtT, 4GGV; HmtN, 5WX2; HmtS, 5Z9I.

[1]Department of Chemistry, Massachusetts Institute of Technology, Cambridge, MA 02139, USA.
*Corresponding author. Email: movassag@mit.edu (M.M.); blp@mit.edu (B.L.P.)

to oxidative tailoring by three cytochrome P450 enzymes (*8*). The final step, catalyzed by HmtS, forges the central C5–C5′ bond by oxidative dimerization of (+)-himastatin monomer (**2**). On the basis of recent theoretical studies of P450-catalyzed C–C bond formation, we envisioned that this enzymatic dimerization may take place via radical–radical coupling of two cyclotryptophan radicals (fig. S2) (*15*, *16*). These radical species are likely generated in rapid succession via indoline N–H hydrogen-atom abstraction at the heme active site, before undergoing combination in its vicinity (*16*, *17*).

We envisioned that a biosynthetically inspired chemical method for the oxidative dimerization of cyclotryptophans could follow the same radical–radical coupling blueprint. As opposed to hydrogen atom abstraction, we planned to generate an analogous open-shell cyclotryptophan species via single-electron oxidation of the embedded aniline substructure. Consistent with studies of aniline dimerization via single-electron oxidation (*18*–*20*), we predicted that the resulting arylamine radical cation would rapidly dimerize at the most accessible position, forming the desired C5–C5′ linkage.

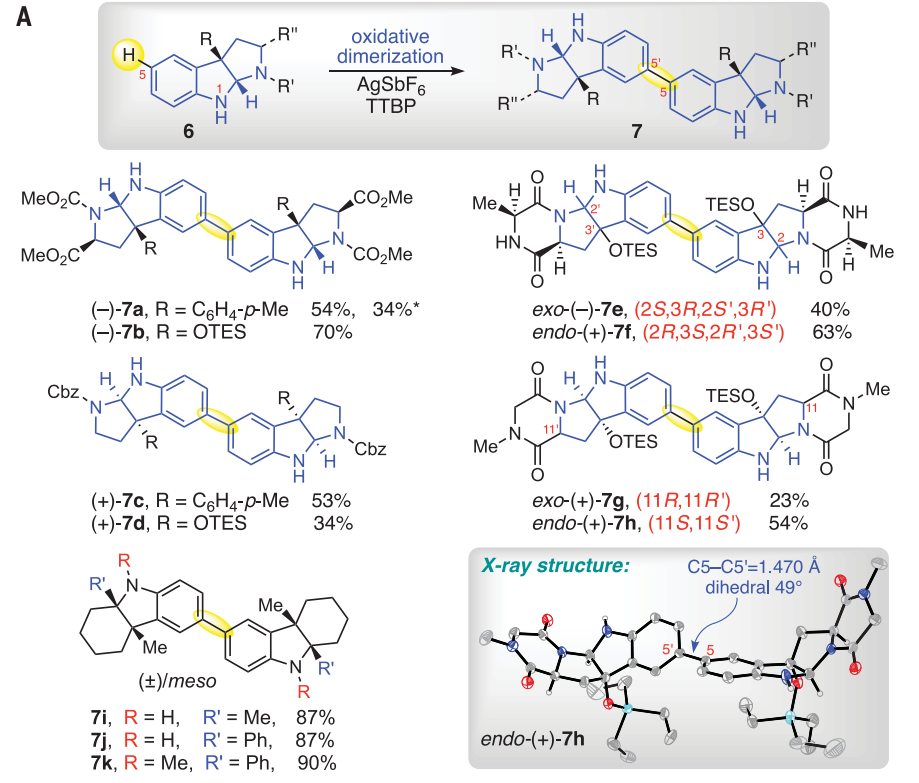

Fig. 2. Oxidative dimerization of cyclotryptophan, cyclotryptamine, and indolines. (**A**) Substrate scope of our oxidative dimerization reaction. In the ORTEP representation of dimeric *endo*-diketopiperazine (+)-**7h**, the thermal ellipsoids are drawn at 30% probability, and only selected hydrogen atoms are shown. (**B**) Mechanistic studies using equimolar mixtures of differentially substituted indolines provide evidence for a radical–radical coupling mechanism. Reagents and conditions: $AgSbF_6$, TTBP, $ClCH_2CH_2Cl$, 23°C; * copper (II)-catalyzed conditions: $Cu(OTf)_2$ (20 mol %), Ag_2CO_3, $ClCH_2CH_2Cl$, 23°C. TES, triethylsilyl; TTBP, 2,4,6-tri-*tert*-butylpyrimidine.

Late-stage application of this chemistry to dimerization of (+)-himastatin monomer (**2**) permits a straightforward modular assembly of linear hexadepsipeptide **5** akin to native precursor **4**, without the constraints imposed by bidirectional elaboration of a simple dimeric cyclotryptophan (*9*, *11*, *12*). Direct union of complex peptide macrocycles also offers the elusive opportunity to access heterodimeric derivatives of (–)-himastatin (**1**).

Our dimerization method required the identification of a single-electron oxidant that would target the aniline substructure within a complex cyclotryptophan precursor (*21*). Existing precedent for the use of inorganic oxidants for generation of aniline radical cations (*20*) ultimately guided our initial selection of reagents. We found that excess silver(I) hexafluoroantimonate [5 equivalents (equiv.)], in combination with the non-nucleophilic pyrimidine base TTBP (*22*) in 1,2-dichloroethane, could effect C5–C5′ dimerization of cyclotryptophan, cyclotryptamine, and indoline derivatives (Fig. 2A). In each case, a single regioisomer consistent with a symmetric C5–C5′ linked homodimer was isolated. Single-crystal x-ray diffraction of dimeric *endo*-diketopiperazine (+)-**7h** verified the expected connectivity. The use of an aqueous sodium thiosulfate reductive workup was critical for optimal isolation of the dimers, as a second equivalent of oxidant is consumed owing to their sensitivity toward further oxidation under the reaction conditions (*23*, *24*). We found that *exo*-configured diketopiperazines **6e** and **6g** were subject to complete oxidation in approximately half the time of their corresponding *endo*-derivatives **6f** and **6h**, respectively. This finding correlates with the increased accessibility of the N1 locus in substrates **6e** and **6g**, the site of initial oxidation (*25*). Substitution of N1 with a methyl group in the case of indoline **6k** did not inhibit the dimerization, consistent with a radical intermediate as opposed to a closed-shell arenium cation (*26*). As part of our optimization efforts (table S1) (*23*) and to expand the range of reagents that could be used in more complex applications of our dimerization method, we also investigated the use of copper(II) salts as single-electron oxidants (*20*). Cyclotryptophan dimer (–)-**7a** could be obtained by using catalytic copper(II) trifluoromethanesulfonate and silver(I) carbonate as the terminal oxidant, albeit in lower yield (34%, 18% recovered starting material) compared to stoichiometric $AgSbF_6$ (54%, 53% on a 0.50-mmol scale).

To investigate the mechanism of this C–C bond–forming dimerization reaction, we devised a series of experiments using indoline substrates (Fig. 2B and fig. S3) (*23*). When an equimolar mixture of C2-methyl and C2-phenyl indolines **6i** and **6j**, respectively, was subjected to our dimerization conditions, we observed a statistical mixture of homo- and heterodimers arising

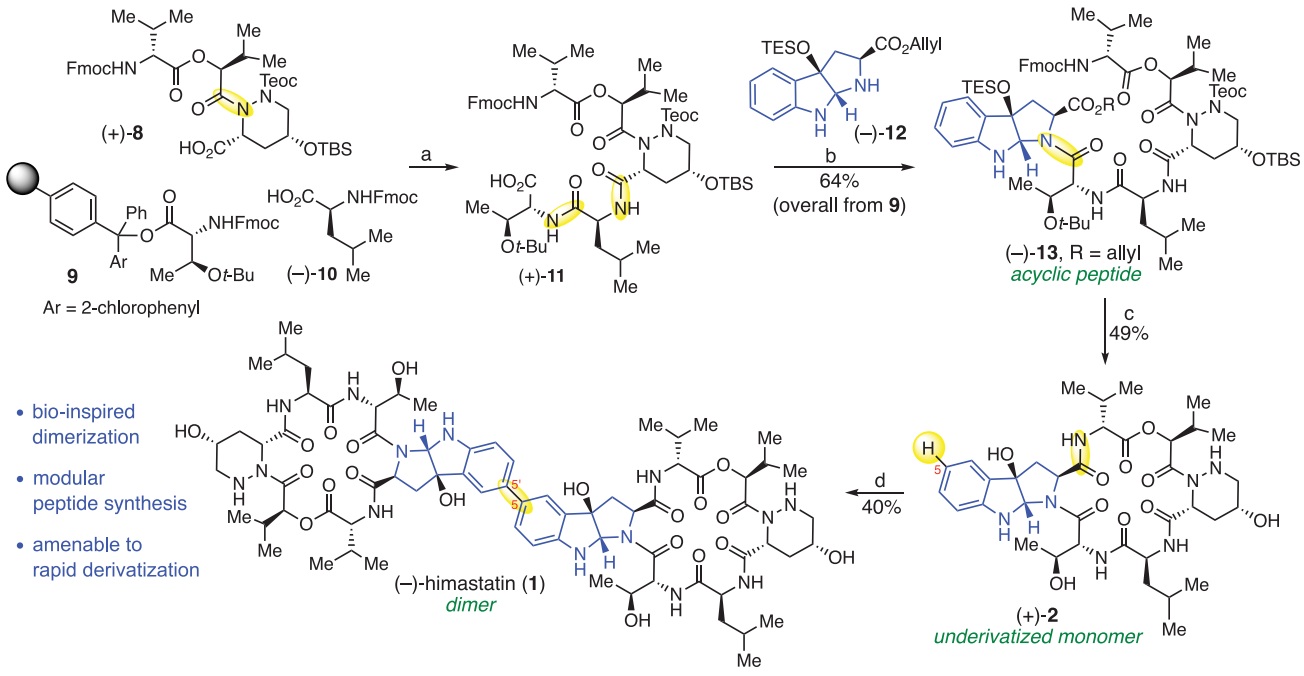

Fig. 3. Concise total synthesis of (–)-himastatin (1). Reagents and conditions: (a) (i) piperidine, DMF, 23°C; (ii) (–)-**10**, HATU, *i*-Pr_2NEt, DMF, 23°C; (iii) piperidine, DMF, 23°C; (iv) (+)-**8**, HATU, *i*-Pr_2NEt, DMF, 23°C; (v) TFA, CH_2Cl_2, 23°C. (b) (–)-**12**, HATU, HOAt, 2,4,6-collidine, CH_2Cl_2, 0 → 23°C. (c) (i) $Pd(PPh_3)_4$, *N*-methylaniline, THF, 23°C; (ii) *i*-Pr_2NH, MeCN, 23°C; (iii) HATU, HOAt, *i*-Pr_2NEt, CH_2Cl_2, 23°C; (iv) TFA, H_2O, anisole; Et_3N, MeOH, 23°C. (d) $Cu(SbF_6)_2$, DTBMP, $ClCH_2CH_2Cl$, 23°C. Ar, 2-chlorophenyl; DMF, *N*,*N*-dimethylformamide; DTBMP, 2,6-di-*tert*-butyl-4-methylpyridine; Fmoc, 9-fluorenylmethoxycarbonyl; HATU, hexafluorophosphate azabenzotriazole tetramethyl uronium; HOAt, 1-hydroxy-7-azabenzotriazole; Leu, leucine; TBS, *tert*-butyldimethylsilyl; Teoc, 2-trimethylsilylethyloxycarbonyl; TFA, trifluoroacetic acid; THF, tetrahydrofuran.

from similar rates of single-electron oxidation (Fig. 2B, green; fig. S3, eq. 1). However, oxidative dimerization of an equal mixture of indolines **6j** and **6k** gave predominantly (90%) homodimer formation, along with a trace (4%) amount of heterodimer **7n** (fig. S3, eq. 2). When a limiting quantity of oxidant was used, we determined that these indoline substrates were consumed sequentially, with N1-methyl indoline **6k** dimerizing selectively over NH indoline **6j** (Fig. 2B, blue, and fig. S3, eq. 3). Having observed homodimerization of a more readily oxidized monomer in the presence of a similarly nucleophilic but less readily oxidized monomer, we conclude that C5–C5′ bond formation preferentially occurs through radical–radical coupling rather than nucleophilic capture. This conclusion is consistent with the absence of adduct formation in the homodimerization of cyclotryptophan **6a** despite the presence of external π-nucleophiles (e.g., methallyltrimethylsilane, dimethylketene silyl acetal, *N*-trimethylsilylindoline) and is reinforced by prior studies demonstrating that radical–radical coupling between aniline radical cations is fast (k = ~10^7 M^{-1}•s^{-1} for the dimerization of $PhNMe_2^{\bullet+}$) (*18*–*20*). We postulate that the high local concentration of radical species near the surface of the oxidant favors their direct combination over nucleophilic pathways (*14*, *20*). In the context of our synthetic efforts, the rapid rate and apparent insensitivity of the radical–radical coupling manifold to nucleophilic interference bode well for the application of this chemistry to complex substrates. These findings highlight a possible underlying parallel between our oxidative dimerization methodology and our mechanistic proposal for the biosynthetic dimerization catalyzed by HmtS (fig. S2), involving successive generation of radical species in close proximity to each other.

For the synthesis of (+)-himastatin monomer (**2**), we sought to leverage the practical advantages of solid-phase peptide synthesis (*27*), offering rapid and customizable access to complex peptides by minimizing repetitive purification and isolation steps. In contrast to the reported solution-based approach to intermediates en route to (–)-himastatin (**1**) (*9*), we relied on a hybrid solution–solid phase synthetic strategy. The resin-bound D-threonine **9** (Fig. 3) was elaborated with L-leucine (–)-**10** and tridepsipeptide fragment (+)-**8**, the latter being prepared in one step (*23*) (78% yield) from a depsipeptide block (*23*, *28*) (three steps from commercial carboxylic acids) and known *N*ε, *O*-protected D-5-hydroxypiperazic acid **S8** (*9*) (nine steps from 4-pentenoic acid). The crude pentadepsipeptide acid (+)-**11** obtained upon cleavage was then coupled with cyclotryptophan (–)-**12** [fig. S4; five steps from commercial tryptophan derivative (–)-**S3**, 60% yield], affording linear hexadepsipeptide (–)-**13** in 64% overall yield from threonine resin **9** (*23*). The efficient hybrid synthetic strategy we have developed enabled convergent assembly of intermediate hexadepsipeptide (–)-**13** with only a single chromatographic purification, which compares favorably to linear solution-phase synthesis, which requires at least 10 separate steps to access an intermediate of similar complexity (*9*). Furthermore, our modular strategy allows for conducting difficult couplings in solution (*28*) and introducing the tryptophan residue as a cyclotryptophan to bypass stereoselectivity concerns that would arise from late-stage oxidation (*29*). Following termini deprotection, linear peptide (–)-**13** was cyclized to (+)-himastatin monomer (**2**) in 49% overall yield (Fig. 3), affording the immediate biosynthetic precursor to (–)-himastatin (**1**). All ^1H and ^{13}C nuclear magnetic resonance (NMR) data, as well as optical rotation for synthetic monomer (+)-**2**, were consistent with literature values (*8*, *9*).

Having accessed (+)-himastatin monomer (**2**), we focused on the application of our biosynthetically inspired oxidative dimerization methodology to complete the total synthesis of (–)-himastatin (**1**) (Fig. 3). Although silver(I) hexafluoroantimonate and copper(II) trifluoromethanesulfonate were effective for the

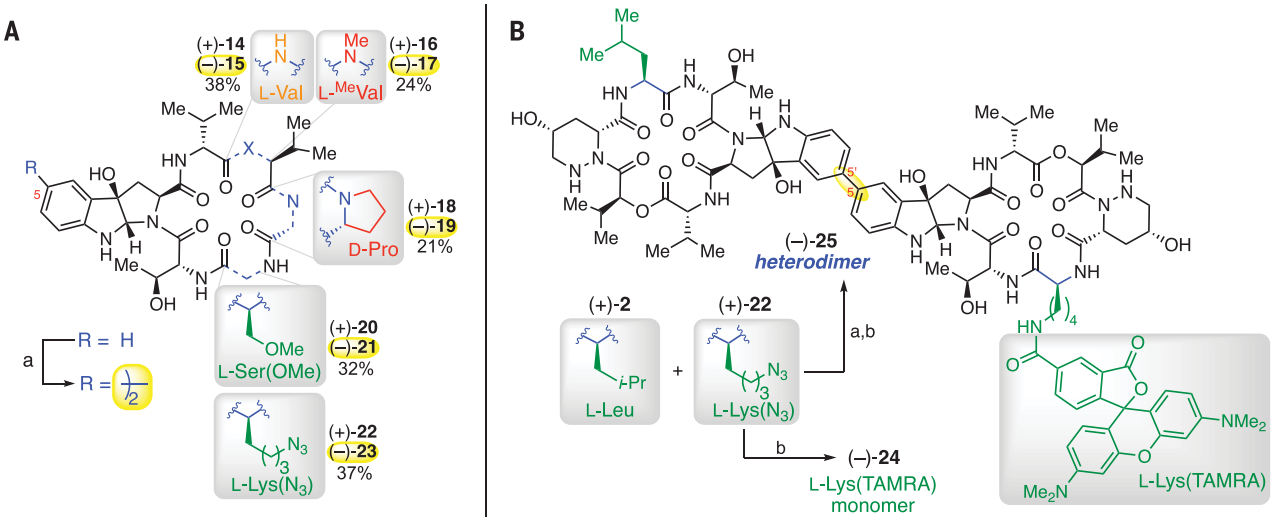

Fig. 4. Synthesis of designed derivatives and probes of himastatin. (**A**) Dimerization of unnatural himastatin derivatives with single-residue substitutions. (**B**) Synthesis of a heterodimeric fluorescent himastatin probe. Reagents and conditions: (a) $Cu(SbF_6)_2$, DTBMP, $ClCH_2CH_2Cl$, 23°C. (b) (i) PMe_3, H_2O, THF, 40°C; (ii) 5-TAMRA succinimidyl ester, *i*-Pr_2NEt, DMF, 23°C. Lys, lysine; Pro, proline; Ser, serine; TAMRA, carboxytetramethylrhodamine; Val, valine.

dimerization of simpler cyclotryptophans (Fig. 2A), they gave little to no oxidation of the cyclotryptophan incorporated within the more complex (+)-himastatin monomer (**2**). We hypothesized that aggregation and inactivation of these insoluble oxidants, combined with the lower reactivity of complex macrocyclic peptide substrates, may be responsible for the low conversion, and we sought to address the challenge posed by evaluating other single-electron oxidants. Consistent with this hypothesis, insoluble oxidants such as other Ag(I,II) and Cu(II) salts were generally ineffective. However, soluble oxidants, including organic radical cations such as magic blue [$(4\text{-BrPh})_3N^{\bullet+}SbF_6$], did provide oxidation, but products derived from nucleophilic substitution of the C–Br bond (S_NAr) by the peptide dominated (*21*). Informed by our prior use of Cu(II) for the dimerization of simpler substrates and in search of an oxidant with both good solubility and low propensity toward nucleophilic capture, we identified copper(II) hexafluoroantimonate. Our isolation of freshly prepared $Cu(SbF_6)_2$, commonly used as a soluble Lewis acid catalyst (*30*), provided us with an opportunity to investigate its use as a stoichiometric oxidant. In the event, exposure of (+)-himastatin monomer (**2**) to excess $Cu(SbF_6)_2$ (20 equiv.) and DTBMP (4 equiv.) in 1,2-dichloroethane afforded (–)-himastatin (**1**) in 40% yield (3 mg), with only trace (<5%) amounts of recovered starting material. The remainder of the mass balance consisted of minor undesired products, including dimers and oligomers. Our convergent synthesis of the natural product (–)-**1** is enabled by the hybrid solution–solid phase assembly of readily available tridepsipeptide (+)-**8**, resin-bound D-Thr **9**, L-leucine (–)-**10**, and cyclotryptophan (–)-**12**, comprising 11 steps (5 on solid-support, 6 in solution) and requiring only three isolations to access (–)-himastatin (**1**) from D-Thr **9** in 13% overall yield. All spectroscopic data, as well as optical rotation, for synthetic (–)-himastatin (**1**) were consistent with literature values (*6*, *9*).

Our concise and versatile chemical synthesis of himastatin, featuring a biosynthetically inspired final-stage dimerization reaction, presented an opportunity both to interrogate structural characteristics that are important for its bioactivity and to access synthetic probes for chemical biology studies (Fig. 4). We hypothesized that the alternating sequence of D,L-residues present in the macrocyclic rings of (–)-himastatin (**1**) could promote self-assembly (*31*, *32*), inspiring our preparation of both the enantiomer (*ent*-(+)-**1**) and *meso* derivative of himastatin (**1**). These stereochemical probes were prepared from precursors of opposite chirality, and in the case of the heterodimer *meso*-himastatin (**1**), by dimerization of an equal mixture of monomer **2** enantiomers and separation of the resulting heterodimer (*23*). Apart from slight variations in the chemical shifts of aromatic ^1H and ^{13}C signals, the spectra of *meso*-himastatin (**1**) were nearly identical to those of the corresponding homodimers. We also selected several derivatives with single-residue substitutions to synthesize, each varying a residue that is specific to himastatin among related antibiotics. In all cases, our modular hybrid peptide synthesis approach was quickly adapted to introduce the substituted residue, and the resulting monomers were effectively dimerized (21 to 37% yield) under the conditions developed for the synthesis of (–)-himastatin (**1**) (Fig. 4A) (*23*). As an orthogonal mechanistic probe that would permit direct visualization of himastatin's interaction with bacteria, we designed a fluorescent heterodimer that we predicted would retain antibiotic activity (see below). TAMRA-himastatin heterodimer (–)-**25** was rapidly prepared through the union of himastatin monomer (+)-**2** and azidolysine monomer (+)-**22** followed by labeling via a reduction–acylation sequence (Fig. 4B). This procedure also provided access to TAMRA-himastatin homodimer (–)-**S17** as a useful control (*23*).

We found that synthetic (–)-himastatin (**1**) showed in vitro antibiotic activity against several Gram-positive species, including antibiotic-resistant strains of public health concern (Table 1 and table S11) (*1*). Our synthetic (–)-himastatin (**1**) showed minimum inhibitory concentration (MIC) values (1 to 2 μg/ml) similar to those reported for natural (–)-himastatin (**1**) in identical species (*4*). All monomeric derivatives prepared in this study had MIC values ≥64 μg/ml across all species tested (*9*, *23*), highlighting the critical role of dimerization for antibiotic activity. Our stereochemical probes revealed that the absolute stereochemistry of himastatin has negligible impact on its antibiotic activity; stereoisomers of himastatin (**1**) were found to have nearly identical MIC values across the *Bacillus subtilis*, *Staphylococcus aureus*, and *Enterococcus faecalis* strains tested. This finding has also been observed among enantiomers of certain membrane-targeting cyclic peptides with alternating stereochemistry (*33*) and is consistent with antibiotic activity depending on achiral as opposed to diastereomeric interactions that would lead to differential activity of each stereoisomer (e.g., with peptides or receptors) (*34*, *35*). By contrast, we found

Table 1. Antibiotic evaluation of himastatin derivatives and probes against Gram-positive bacteria. MIC values were determined by using the broth-microdilution method; see table S11. MRSA, methicillin-resistant *Staphylococcus aureus*; MSSA, methicillin-sensitive *S. aureus*; VRE, vancomycin-resistant *Enterococcus*; VSE, vancomycin-sensitive *Enterococcus*.

		MIC (μg/ml)		MIC (μg/ml)					
Compound	**Monomer**	***B. subtilis***	**Dimer**	***B. subtilis***	**MRSA**	**MSSA**	**VRE *faecalis***	**VSE *faecalis***	***S. himastatinicus***
(−)-himastatin	(+)-**2**	>64	(−)-**1**	1	2	1	1	1	8
ent-(+)-himastatin	(−)-**2**	>64	(+)-**1**	0.5	2	2	2	1	1
meso-himastatin	–	–	*meso*-**1**	1	2	1	1	1	4
rac-himastatin	(±)-**2**	>64	(±)-**2**	0.5	2	2	1	1	2
			Single-residue substitutions						
L-Val	(+)-**14**	>64	(−)-**15**	8	64	16	32	16	>64
L-^{Me}Val	(+)-**16**	>64	(−)-**17**	>64	>64	>64	>64	>64	>64
D-Pro	(+)-**18**	>64	(−)-**19**	>64	>64	>64	>64	>64	>64
L-Ser(OMe)	(+)-**20**	>64	(−)-**21**	2	4	4	1	2	8
L-Lys(N_3)	(+)-**22**	>64	(−)-**23**	2	2	2	2	1	8
L-Lys(TAMRA)	(+)-**24**	>64	(−)-**25**	6	>64	>64	16	16	–

that *ent*-(+)-himastatin (**1**) was four- to eight-fold more active in inhibiting the growth of the producing organism, *Streptomyces himastatinicus*, compared with (−)-himastatin (**1**). This finding might be explained by the presence of known self-resistance mechanisms that have evolved in other species, such as enzymatic degradation and efflux, which would be expected to show differences between stereoisomers (*36*).

The introduction of a strategically positioned functional handle in (−)-himastatin (**1**) was a key goal of our derivative design that would permit introduction of a fluorescent tag. We focused on L-leucine substitution, given the natural variation of this site among related antibiotics (fig. S1). Replacement with an *O*-methyl serine residue [L-Ser(OMe), dimer (−)-**21**], which is found in (−)-chloptosin (**S1**), had minimal impact on antibiotic activity. A similar finding was observed upon substitution with L-azidolysine [L-Lys(N_3), dimer (−)-**23**], which offered the conjugation site exploited in our synthesis of fluorescent probes. However, unlike serine and azidolysine homodimers (−)-**21** and (−)-**23**, respectively, the corresponding TAMRA-himastatin homodimer (−)-**S17** was inactive (MIC > 64 μg/ml) (fig. S5 and table S11). In addition to TAMRA, homodimeric himastatin analogs derived from other fluorophores were also found to be inactive (fig. S5). Consistent with our expectation that minimizing the overall perturbation of himastatin's structure to only one half of the dimer may preserve antibiotic activity, we found that the MIC of TAMRA-heterodimer (−)-**25** (Fig. 4B) was indeed comparable to that of (−)-himtastatin (**1**) in *B. subtilis* (6 versus 1 μg/ml). Thus, the opportunity for heterodimer formation offered by our biogenetically inspired late-stage dimerization methodology was instrumental to secure access to a fluorescent himastatin probe (*37*), as well as other key derivatives including *meso*-himastatin (**1**) that would otherwise be challenging to prepare by chemoenzymatic or bidirectional synthesis (*9*, *10*).

Other structural features specific to (−)-himastatin (**1**) include a depsipeptide linkage and 5-hydroxypiperazic acid residue. Evaluating the derivatives that we prepared to study these particular structural features, we observed a trend of decreasing antibiotic activity when the ester linkage was replaced with either a secondary amide (−)-**15** or tertiary amide (−)-**17**, consistent with the loss of a hydrogen-bond site (*38*). Furthermore, when the 5-hydroxypiperazic acid residue was replaced with a proline residue, antibiotic activity was completely abolished. Although proline residues are known to induce turn formation, especially when the adjacent amino acid is of opposite α-stereochemistry, they do not exhibit a rigidifying effect as pronounced as that seen in *N*-acyl piperazic acid derivatives (*39*). Consistent with the predicted loss of rigidity upon proline substitution, NMR spectra of homodimer (−)-**19** and monomer (+)-**18** in various solvents at 23°C revealed the presence of minor conformers not observed in the spectra of (−)-himastatin (**1**) or our other derivatives. Taken together, these results provide evidence that structural rigidity, enforced by hydrogen-bonding and conformational restriction, is important to himastatin's antimicrobial mode of action.

Confocal microscopy has been used to observe the biological effects of antibiotics on *B. subtilis*, including the first approved membrane-disrupting lipopeptide, daptomycin (*37*). We sought to use our synthetic compounds in conjunction with this experimental approach to further characterize the antibiotic activity of (−)-himastatin (**1**). Our synthetic heterodimeric probe, TAMRA-himastatin (−)-**25**, offered an opportunity to directly visualize its interaction with bacteria and monitor cellular localization. When *B. subtilis* cells were treated with either 8 or 16 μg of TAMRA-himastatin (−)-**25** per milliliter of solution, we observed substantial accumulation in the bacterial envelope (fig. S6A), with little to no intracellular staining seen at the lower concentration. More cells were stained with TAMRA-himastatin (−)-**25** at the lower concentration than at the higher, but a smaller proportion of the stained cells exhibited visible membrane defects (*23*). The most intense sites of staining were observed at bacterial septa, in addition to patches of stain along sidewalls. At the higher concentration (fig. S6B), defects such as membrane extrusions coincided with lateral accumulation of TAMRA-himastatin (−)-**25**. These sites of curvature appear to reflect areas where the antibiotic has induced changes to membrane morphology.

The staining pattern observed with TAMRA-himastatin (−)-**25** was similar to that of the membrane stain FM4-64 with unmodified himastatin (**1**) (fig. S7). Untreated *B. subtilis* cells have smooth membranes and normal septal rings, but cells treated with a sublethal concentration of either enantiomer of himastatin (**1**) display pronounced membrane defects, notably patches of membrane thickening. Furthermore, the observed similarity in membrane morphology between himastatin (**1**) enantiomers appears to be consistent with

their similar antibiotic activity. In a separate experiment, we evaluated the time scale by which (–)-himastatin (**1**) acts on bacteria at lethal concentrations (fig. S8). When treated with (–)-himastatin (**1**) at a concentration twice the MIC value, bacterial membranes were permeabilized within 30 min, as indicated by influx of the viability stain SYTOX Green.

The observations of our microscopy studies are comparable to those seen with daptomycin despite a lack of structural similarity to himastatin (*37*). The membrane defects and localization patterns observed in *B. subtilis* with unmodified (–)-himastatin (**1**) and our fluorescent himastatin derivative (–)-**25** show resemblance to those seen with unmodified and fluorescent forms of daptomycin, respectively (*37*). Furthermore, the short time scale of membrane permeabilization following treatment with himastatin (**1**), like that seen after treatment with daptomycin, is consistent with a mode of action based on physical perturbations (*33*, *37*). This mode of action is distinct from that of certain other Gram-positive peptide antibiotics, such as vancomycin and teixobactin, that interfere with cell-wall biosynthesis and have kill times longer than 30 min (*40*). Separately, the similarity in MIC values and cellular morphology among our series of synthetic himastatin stereoisomers reveals that achiral interactions—for example, with the hydrophobic groups of phospholipids (*34*, *35*)—are largely responsible for the observed antibiotic activity. In summary, our chemical biology studies using our synthetic probes offer findings that are consistent with the hypothesis that (–)-himastatin's (**1**) antibiotic activity is dependent on interaction with bacterial membranes (*7*). It is evident that (–)-himastatin (**1**) is a distinct member among known membrane disruptors (*41*).

Published preclinical studies of (–)-himastatin's (**1**) biological activity are limited to early reports primarily focused on its antitumor activity (*4*, *7*). For instance, it was found that intraperitoneal administration of (–)-himastatin (**1**) prolonged the life span of mice inoculated with leukemia or melanoma cells, with toxicity being observed at the highest doses evaluated (*4*). Against the backdrop of escalating antibiotic resistance, we aim to continue detailed study and evaluation of (–)-himastatin's (**1**) antibiotic activity and application of new insights in the rational design and synthesis of analogs with improved characteristics.

REFERENCES AND NOTES

1. H. W. Boucher *et al*., *Clin. Infect. Dis.* **48**, 1–12 (2009).
2. C. L. Ventola, *P&T* **40**, 277–283 (2015).
3. G. D. Wright, *Can. J. Microbiol.* **60**, 147–154 (2014).
4. K. S. Lam *et al*., *J. Antibiot.* **43**, 956–960 (1990).
5. J. E. Leet, D. R. Schroeder, B. S. Krishnan, J. A. Matson, *J. Antibiot.* **43**, 961–966 (1990).
6. J. E. Leet *et al*., *J. Antibiot.* **49**, 299–311 (1996).
7. S. W. Mamber *et al*., *Antimicrob. Agents Chemother.* **38**, 2633–2642 (1994).
8. J. Ma *et al*., *Angew. Chem. Int. Ed.* **50**, 7797–7802 (2011).
9. T. M. Kamenecka, S. J. Danishefsky, *Chemistry* **7**, 41–63 (2001).
10. Z. Guo *et al*., *J. Am. Chem. Soc.* **140**, 18009–18015 (2018).
11. S.-M. Yu, W.-X. Hong, Y. Wu, C.-L. Zhong, Z.-J. Yao, *Org. Lett.* **12**, 1124–1127 (2010).
12. A. J. Oelke *et al*., *Chemistry* **17**, 4183–4194 (2011).
13. J. Kim, J. A. Ashenhurst, M. Movassaghi, *Science* **324**, 238–241 (2009).
14. M. Movassaghi, O. K. Ahmad, S. P. Lathrop, *J. Am. Chem. Soc.* **133**, 13002–13005 (2011).
15. J. M. Grandner, R. A. Cacho, Y. Tang, K. N. Houk, *ACS Catal.* **6**, 4506–4511 (2016).
16. R. H. Takahashi *et al*., *Drug Metab. Dispos.* **48**, 521–527 (2020).
17. V. V. Shende *et al*., *J. Am. Chem. Soc.* **142**, 17413–17424 (2020).
18. D. Larumbe, I. Gallardo, C. P. Andrieux, *J. Electroanal. Chem. Interfacial Electrochem.* **304**, 241–247 (1991).
19. H. Yang, D. O. Wipf, A. J. Bard, *J. Electroanal. Chem.* **331**, 913–924 (1992).
20. M. Kirchgessner, K. Sreenath, K. R. Gopidas, *J. Org. Chem.* **71**, 9849–9852 (2006).
21. N. G. Connelly, W. E. Geiger, *Chem. Rev.* **96**, 877–910 (1996).
22. D. Crich, M. Smith, Q. Yao, J. Picione, *Synthesis* **2001**, 323–326 (2001).
23. See supplementary materials.
24. O. Ivashenko, J. T. van Herpt, P. Rudolf, B. L. Feringa, W. R. Browne, *Chem. Commun.* **49**, 6737–6739 (2013).
25. B. M. Nelson, R. P. Loach, S. Schiesser, M. Movassaghi, *Org. Biomol. Chem.* **16**, 202–207 (2018).
26. P. G. Gassman, G. A. Campbell, R. C. Frederick, *J. Am. Chem. Soc.* **94**, 3884–3891 (1972).
27. J. S. Albin, B. L. Pentelute, *Aust. J. Chem.* **73**, 380–388 (2020).
28. M. M. Nguyen, N. Ong, L. Suggs, *Org. Biomol. Chem.* **11**, 1167–1170 (2013).
29. K. L. Greenman, D. M. Hach, D. L. Van Vranken, *Org. Lett.* **6**, 1713–1716 (2004).
30. S.-K. Chang, P. Selvaraj, "Copper(II) Hexafluoroantimonate" in *Encyclopedia of Reagents for Organic Synthesis* (Wiley, 2005), pp. 1–4.
31. P. De Santis, S. Morosetti, R. Rizzo, *Macromolecules* **7**, 52–58 (1974).
32. L. Tomasic, G. P. Lorenzi, *Helv. Chim. Acta* **70**, 1012–1016 (1987).
33. S. Fernandez-Lopez *et al*., *Nature* **412**, 452–455 (2001).
34. D. Wade *et al*., *Proc. Natl. Acad. Sci. U.S.A.* **87**, 4761–4765 (1990).
35. C. K. Wang *et al*., *J. Am. Chem. Soc.* **138**, 5706–5713 (2016).
36. E. Peterson, P. Kaur, *Front. Microbiol.* **9**, 2928 (2018).
37. J. Pogliano, N. Pogliano, J. A. Silverman, *J. Bacteriol.* **194**, 4494–4504 (2012).
38. Y. Li *et al*., *ACS Med. Chem. Lett.* **8**, 1171–1176 (2017).
39. N. Xi, L. B. Alemany, M. A. Ciufolini, *J. Am. Chem. Soc.* **120**, 80–86 (1998).
40. L. L. Ling *et al*., *Nature* **517**, 455–459 (2015).

ACKNOWLEDGMENTS

We thank W. C. Salmon at the W. M. Keck Microscopy Facility (Whitehead Institute) for assistance with confocal microscopy; C. Tsay and P. Müller (Massachusetts Institute of Technology) for assistance with single-crystal x-ray diffraction of (+)-**7h**; and R. P. Bhattacharyya (Massachusetts General Hospital) for providing several bacterial strains. We are grateful to J. S. Albin (Massachusetts General Hospital) for helpful discussions.
Funding: This study was supported by NIH grants GM-089732 and GM-141963 (M.M.); an NSERC postgraduate scholarship, grant PGSD3-502869-2017 (K.A.D.); and an NSF graduate research fellowship, grant 1122374 (C.K.S.). **Author contributions:** K.A.D. and M.M. conceived the project and designed the synthetic routes; K.A.D. performed the chemical synthesis; C.K.S. performed the antibiotic assays and fluorescence microscopy; all coauthors wrote and edited the manuscript. **Competing interests** A patent application covering this work has been filed by MIT (US patent application no. 63/153,286). **Data and materials availability:** Experimental procedures, spectroscopic data, and copies of NMR spectra are available in the supplementary materials. Structural parameters for *endo*-diketopiperazine (+)-**7h** are freely available from the Cambridge Crystallographic Data Centre under CCDC-2099734.

SUPPLEMENTARY MATERIALS

science.org/doi/10.1126/science.abm6509
Materials and Methods
Figs. S1 to S13
Tables S1 to S11
References (*41*–*49*)
Spectral Data

1 October 2021; accepted 21 December 2021
10.1126/science.abm6509

Total synthesis of himastatin

Kyan A. D'AngeloCarly K. SchisselBradley L. PenteluteMohammad Movassaghi

Science, 375 (6583), • DOI: 10.1126/science.abm6509

A late coupling for himastatin

Himastatin is a bacterial natural product that has been studied over the past several decades for its antibiotic properties and intriguing structure. The compound is a dimer of peptide macrocycles linked through a bond between the aryl rings of two cyclotryptophan residues. D'Angelo *et al*. report a comparatively efficient synthesis of himastatin as well as its unnatural enantiomer and several other derivatives (see the Perspective by Smith). The key step is a late-stage dimerization relying on oxidation of the monomers by a copper salt. Fluorescent tagging sheds light on the compound's cell membrane–disrupting mechanism of action. —JSY